5

Abundance of F in stars of GC M4, M22, 47 Tuc and NGC 6397

5.1 Introduction

The presence of ^{19}F which has been confirmed by observation is of the essence in all the four GCs namely M4 (Smith et al. 2005; Sánchez-Blázquez et al. 2012[285])), M 22 (Alves-Brito et al. 2012[275]); D'Orazi et al. 2013[278])), NGC 6397 and 47 Tuc (de Laverny et al. 2013[276])) as well. Recently, Abia et al. 2010[274]) have even confirmed the presence of

^{19}F in galactic AGB stars. This ^{19}F is an interesting element of the periodic table because of the fact that though it is surrounded by some of the most abundant elements in the universe like oxygen, nitrogen and neon, after hydrogen and helium yet it is itself very rare. Perhaps it is because an odd Z element with only one single stable isotope and it is very fragile with its 9 protons and 10 neutrons (Palacois 2006). However the origin of ^{19}F is still a matter of debate. The three proposed primary astrophysical factories for ^{19}F production have been the Type II supernovae (SNe II), the Wolf-Rayet (WR) stars, and the asymptotic giant branch (AGB) stars (Renda et al. 2004[284]); Recio-Blanco et al. 2012[283])). Each of them has different ^{19}F synthesizing mode. SNe II produces ^{19}F primarily as the result of spallation of ^{20}Ne by ν_μ and ν_τs near the collapsed core. In WR stars ^{19}F production is tied to the nuclear burning chain given by $^{14}N(\alpha,\gamma)^{18}F(\beta^+)^{18}O(p,\alpha)^{15}N(\alpha,\gamma)^{19}F$ (Lucatello et al. 2011[280])). In the case of AGB stars, the reaction network $^{14}N(n,p)^{14}C(\alpha,\gamma)^{18}O(p,\alpha)^{15}N(\alpha,\gamma)^{19}F$ where the neutrons are provided by $^{13}C(\alpha,n)^{16}O$ and the protons mainly by $^{14}N(n,p)^{14}C$ ie it is the combined H and He-burning in the case of AGB stars that produces ^{19}F (Renda et al. 2004[284]); Lucatello et al. 2011[280])). The thermonuclear burning phases, are liable for the synthesis of various elements. One such thermonuclear H-burning scheme that plays an important role in the abundance of elements in the surface layers of stars is the CNO cycle outlined in Chapter 1. However we have chosen the same CNOF cycle, which leads us to get to the element ^{19}F mentioned in the last chapter. This chapter is dedicated to enhance our understanding and additionally to appear for brand spanking new mechanisms of fluorine production in the GC stars.

5.2 Evolutinary scenario: The Basic Physical Situation

In the canonical model of the star discussed in Section 4.3, the synthesized materials are brought to the surface by means of convection, which is the only the mixing mechanism with the convective regions getting fully mixed. In evolved stars there are also some dredging up

episodes which effectively works as far as alteration of elements is concerned. But in case of RGB star canonical extra mixing will not change the surface abundances unless it switches to an enhanced mode. This could result from tidal spin-up of upper RGB stars in close binaries (Denissenkov 2006[277])). Another possibility is that canonical extra mixing gets enhanced toward the RGB tip due to some internal physical processes in single stars. This extra mixing in upper RGB stars can penetrate the H burning shell and from proton mixing (“partial mixing") into the He-rich intershell which is also necessary to activate the s-process in those stars (Mowlavi et al. 1998[282])), may trigger further burning to primary sources like ^{14}N and ^{13}C and ^{16}O along with ^{12}C because partial He burning in the He intershell converts He into ^{12}C (Lugaro et al. 2004[281])) can be added to make the total sum of C+N+O is constant to high accuracy for all stars studied (Smith et al. 2005[288])) to yield the observed abundance of ^{19}F. However we donot comment on the physical factors that influence the mixing or dredging up mechanisms.

5.3 ^{19}F production

Here we took the same nuclear burning cycle as discussed in the last chapter. Initialisation of CNO cycle from ^{12}C(p,γ)^{13}N will eventually lead to the production of ^{14}N from ^{13}C.

^{14}N(p,γ)^{15}O: The experiment performed by the LUNA collaboration (Cristallo et al. 2014[289] and ref. therein) has reached the lowest energy, about 70 keV, which corresponds to a stellar temperature of about T_9=0.05 K. However the uncertainty on data at high energy affects the low energy extrapolation. The CN cycling will be guaranteed as (p,α) reaction wins over the (p,γ) reaction.

^{15}N(p,α)^{12}C: The reaction rate of this process, at the temperatures of interest for this study, is mostly determined by a resonance at $E_{cm} \sim 100$ keV. A decade ago, this reaction has been investigated using the indirect approach of the Trojan Horse Method, THM), (La Cognata et al. 2007[290]), yielding results similar to (Redder et al. (1982)[291]). For the present

work we use the reaction rate reported in the NACRE database. The uncertainty at relevant temperatures is about 10%. Then the presence of branching will also direct towards a (p,γ) reaction.

^{15}**N**(p,γ)^{16}**O**: The low energy cross section of this process is determined by the presence of two broad resonances and by their interference. La Cognata et al. (2009)[292] suggested a cross section significantly lower than previously estimated. This translates into a significantly lower rate at AGB temperatures. In the present work we use the rate presented in NACRE database, and the corresponding uncertainty at relevant temperatures is about 10%.

^{16}**O**(p,γ)^{17}**F**: This reaction was given much emphasis on the stellar temperature range of $0.06 \leq T_9 \leq 0.1$ whichis important for hot bottom burning in asymptotic giant branch (AGB) stars. However the two resonances at E_{cm} = 2.50 and 3.26 MeV (Tilley et al. 1993)[293]) are negligible for the total rate. The reaction rate uncertainties involved, are about 7% over the entire temperature region of astrophysical interest (T_9 = 0.01-2.5 K) (Iliadis et al. (2010)[133]).

^{17}**O**(p,α)^{14}**N**: The reaction rate determination for this reaction, at the astrophysically relevant energy is relatively difficult and the uncertainty is correspondingly large due to the presence of the E_{cm} = 65 keV resonance. The uncertainty at relevant temperatures is about 20%.

^{17}**O**(p,γ)^{18}**F**: The cross section of this reaction below $E_{cm} \approx$ 400 keV is determined by 2 narrow resonances. Chafa et al. (2007)[294]; Newton et al. (2010)[295] have determined the reaction rate with improving precision. Nevertheless, at the temperatures relevant for AGB nucleosynthesis, the reaction rate is dominated by the lowest energy resonance, E_{cm} = 65 keV, that is too weak to be directly measured with the current experiment possibilities.

^{18}**O**(p,γ)^{19}**F**: In this case the presence of several low energy states influences the determination of the cross section. In particular, the E_{cm} = 150 keV broad resonance and the direct capture dominate the reaction rate at the astrophysically relevant temperature for AGB nucleosynthesis. The uncertainty at relevant temperatures is about 10%.

^{19}F(p,α)^{16}O: Then the finally produced ^{19}F which is destroyed by a (p,α) reaction forming ^{16}O since (p,α) reaction rate is faster as compared to (p,γ) reaction which would have produced ^{20}Ne. It is to be noted that (p,α) situation contains branching. The branching ratio between the α_0, α_π and α_γ outgoing channels in the ^{19}F(p,α)^{16}O reaction are still largely uncertain at astrophysical energies, pointing out the need for new, more comprehensive, measurements. The most recent experimental work on this subject performed by La Cognata et al. (2011)[296], suggesting that at the lowermost energies (T_9 <0.1 K) the α_0 channel dominates in the other open reaction channels (i.e. α_π and α_γ). Moreover, the presence of very low energy resonance at E_{cm} = 300 keV, which was not observed before in direct measurement, until La Cognata et al. (2011)[296]) observed this in an indirect experiment using the THM corresponding to typical AGB temperatures, thus implying a significant increase of the reaction rate. For example at temperatures up to $T_9 \sim 0.05$, where the reaction rate is 27% higher than in NACRE which even increases upto a factor of 1.7 ($T_9 \sim 0.1$). Here in this work we have compared both the reaction rates from the NACRE and La Cognata et al. (2011)[296] and have looked for the extent up to which the ^{19}F abundance alteration has taken place. As far as the realistic astrophysical situation is concerned the reaction rate constants taken here conform to the conditions encountered in red giants, AGB stars, classical novae, massive stars and type I x-ray bursts (Iliadis et al. 2010[133]) and the same from the NACRE comply with the non-explosive H- and He-burning modes with the extrapolation of astrophysical S-factors to very low energies based on potential models (Xu et al. 2013)[297]. There is also production of α-particles taking place in the cycle. Although it looks at first sight that these α particles may also get involved in some (α,γ) type of reactions which can lead to additional branching points in the reaction networks creating some alteration in the abundance profile of the elements. We have calculated the α- capture lifetimes for all the stable elements using an equation similar to the Eq.(4.1) where X_p has been replaced by X_{He} for ρ_2 being the density in units 10^2 g/cm^3. The rate constants for $^{12}C(\alpha,\gamma)^{16}$O,

$^{13}C(\alpha,\gamma)^{17}$O, $^{14}N(\alpha,\gamma)^{18}$F, $^{15}N(\alpha,\gamma)^{19}$F, $^{16}O(\alpha,\gamma)^{20}$Ne, $^{17}O(\alpha,\gamma)^{21}$Ne, $^{18}O(\alpha,\gamma)^{22}$Ne, $^{19}F(\alpha,\gamma)^{23}$Na reactions are taken from the NACRE. The estimated values of the α-capture are shown in the Table (5.1) and in the next one. Then there is also some possibilities of (α,p) type reactions mainly by the nuclei ^{14}O and ^{18}F where the former goes to ^{17}F and the later goes to ^{21}Ne. However these possibilities can also be safely ignored as the α-capture lifetimes still remain large enough even at $T_9 = 0.1$. For instance $^{14}O(\alpha,p)^{17}$F has a median rate constant due to NACRE of magnitude 8.818×10^{-22} cm^{-3}mol^{-1}sec^{-1} which gives a lifetime of 1.62×10^{19} sec according to the Eq.(4.1). For $^{18}F(\alpha,p)^{21}$Ne also we find a lifetime of 4.324×10^{19} sec corresponding to a rate constant 3.304×10^{-22} cm^{-3}mol^{-1}sec^{-1} at $T_9 = 0.1$. We noticed that these α- capture lifetimes are much larger than the typical GC lifetime which is in order of billion years. For instance a recent work by a group of people Hansen et al. 2013[279] have shown that the age of 47 Tuc is 9.7 ± 0.4 Gyr ($\approx 3.15 \times 10^{17}$ sec) and the age of NGC 6397 is 11.7 ± 0.3 Gyr ($\approx 4 \times 10^{17}$ sec) which is still smaller than many α- capture reactions even at $T_9 = 0.1$. Thus the possibility of α- capture can safely be ignored in the calculation, in the adopted range of temperature. The Fig.(5.1) shows a comparative view of p-capture and α- capture lifetimes for the elements involved in the cycle.

Table 5.1 α capture lifetimes τ_α (sec) for various nuclear reactions.

Reaction	T_9	$N_A < \sigma v >$	$\tau_\alpha(\rho_2 = 1)$
$^{12}C(\alpha,\gamma)^{16}$O	0.02	9.86×10^{-33}	3.62×10^{30}
	0.03	4.81×10^{-31}	7.42×10^{28}
	0.05	1.20×10^{-27}	2.97×10^{25}
	0.08	7.43×10^{-23}	4.80×10^{20}
	0.1	1.15×10^{-20}	3.10×10^{18}
$^{13}C(\alpha,\gamma)^{17}$O	0.02	2.30×10^{-46}	1.55×10^{44}
	0.03	1.01×10^{-39}	3.53×10^{37}
	0.05	1.97×10^{-26}	1.81×10^{24}
	0.08	7.62×10^{-22}	4.68×10^{19}
	0.1	8.69×10^{-19}	4.11×10^{16}
$^{14}N(\alpha,\gamma)^{18}$F	0.02	3.27×10^{-48}	1.09×10^{46}
	0.03	5.51×10^{-41}	6.48×10^{38}
	0.05	3.77×10^{-33}	9.47×10^{30}
	0.08	2.77×10^{-26}	1.28×10^{24}
	0.1	2.12×10^{-21}	1.68×10^{19}
$^{15}N(\alpha,\gamma)^{19}$F	0.02	1.70×10^{-46}	2.10×10^{44}
	0.03	3.08×10^{-39}	1.16×10^{37}
	0.05	2.19×10^{-31}	1.63×10^{29}
	0.08	3.71×10^{-25}	9.62×10^{22}
	0.1	2.83×10^{-21}	1.26×10^{19}
$^{16}O(\alpha,\gamma)^{20}$Ne	0.02	1.56×10^{-52}	2.28×10^{50}
	0.03	1.32×10^{-44}	2.70×10^{42}
	0.05	4.66×10^{-36}	7.66×10^{33}
	0.08	2.11×10^{-29}	1.69×10^{27}
	0.1	1.33×10^{-26}	2.68×10^{24}
$^{17}O(\alpha,\gamma)^{21}$Ne	0.02	2.74×10^{-46}	1.30×10^{44}
	0.03	2.35×10^{-38}	1.52×10^{36}
	0.05	8.28×10^{-30}	4.31×10^{27}
	0.08	3.58×10^{-23}	9.97×10^{20}
	0.1	2.19×10^{-20}	1.63×10^{18}
$^{18}O(\alpha,\gamma)^{22}$Ne	0.02	3.22×10^{-48}	1.10×10^{46}
	0.03	2.89×10^{-41}	1.23×10^{39}
	0.05	4.49×10^{-30}	7.95×10^{27}
	0.08	8.84×10^{-24}	4.04×10^{21}
	0.1	5.25×10^{-21}	6.80×10^{18}
$^{19}F(\alpha,\gamma)^{23}$Na	0.02	6.32×10^{-63}	5.65×10^{60}
	0.03	5.96×10^{-54}	5.99×10^{51}
	0.05	5.29×10^{-34}	6.75×10^{31}
	0.08	1.76×10^{-29}	2.02×10^{27}
	0.1	3.93×10^{-25}	9.08×10^{22}

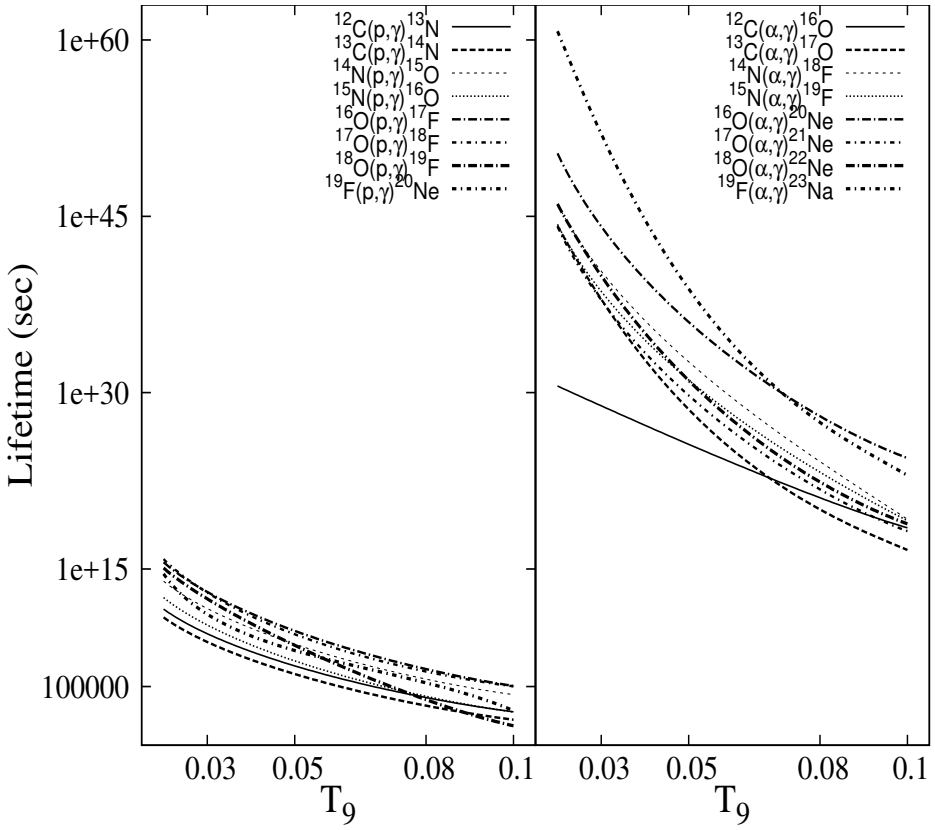

Fig. 5.1 The (α,γ) reactions have lifetimes greater than billion years.

5.3.1 Calculation of ^{19}F abundance

All the reactions are converted into the format of Eq.(4.5) which are basically nothing but eight simultaneous linear first order differential equations, then solved numerically using computer software for the cycle varying the hydrogen mass fraction to $X_H = 0.4$ to get the equilibrium mass fraction abundances of ^{19}F for five different initial conditions. We assume that the heavy elements mass fraction has been shared equally by ^{12}C and ^{16}O. Thus starting with the initial condition to be as the universal one ie $X_H = 0.70$, $X_{He} = 0.28$, $X_{he}(X_{^{12}C} = X_{^{16}O} = 0.01) = 0.02$ such that $X_H + X_{He} + X_{he} = 1$ we have changed the only the heavy element's mass fraction to $X_{he} = 0.01$ $(X_{^{12}C} = X_{^{16}O} = 0.005)$, $X_{he} = 0.002$, $(X_{^{12}C} = X_{^{16}O} = 0.001)$,$X_{he} = 0.001$ $(X_{^{12}C} = X_{^{16}O} = 0.0005)$ upto $X_{he} = 0.0002$ $(X_{^{12}C} = X_{^{16}O} = 0.0001)$

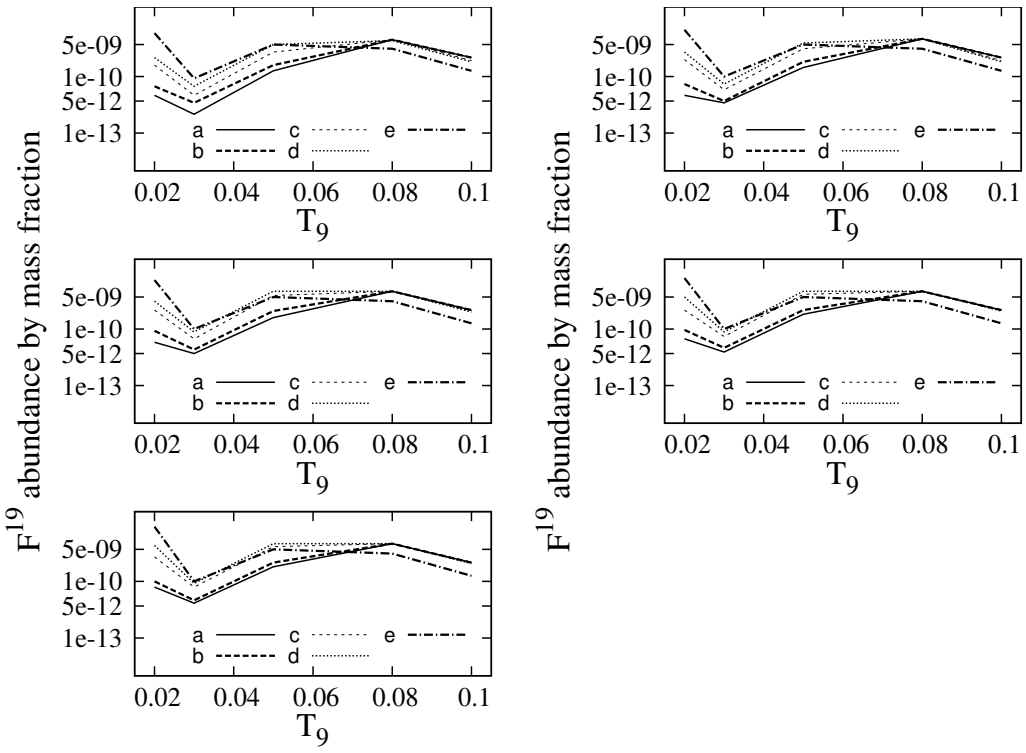

Fig. 5.2 The ^{19}F abundance shown as a function of temperature(T_9) at different hydrogen mass fractions.

keeping only the hydrogen mass fraction fixed. We estimated the equilibrium abundance by mass fraction of ^{19}F which are taken up to the first significant place. These abundance patterns are plotted in Fig.(5.2). As far as the uncertainty in the mass fraction of ^{19}F is concerned we have calculated the same at both low and high reaction rate of the individual reactions taken from (Iliadis et al. 2010[133]) and the NACRE. The ^{19}F abundance grows as T_9 rises but after $T_9 \geq 0.08$ its abundance have shown some decrement. This may be because there are other elements present too in the cycle which abundance might have shown alteration after that temperature. Moreover at larger temperature the ^{19}F destruction via (p,α) reaction deviates from non-resonant to resonant behaviour leading to an enhanced raection rate. Thus as time passes hydrogen will be consuming more and more and it will get depleted. This alteration in hydrogen mass fraction are going to be mirrored within the abundance values of alternative significant heavy elements beside ^{19}F additionally. From

Fig.(5.2) it is seen the mass fraction abundance values of ^{19}F of all the five figures at a given value of X_H, increases with rise in temperature upto $T_9 \leq 0.08$. We have looked for possible alteration of ^{19}F abundance for both NACRE and La Cognata et al. (2011)[296]. For $T_9 = 0.08$ onwards it is seen that as T_9 rises the equilibrium abundance by mass fraction of ^{19}F gets depleted to a lower value as compared to the cases of $T_9 = 0.08$. At temparature ($T_9 \leq 0.08$), the ^{19}F abundance is not found out to be deviating more the 8% for initial condition $Z \sim 5 \times 10^{-4}$. However for temperature ($T_9 \geq 0.08$) and at even lower metallicity $Z \sim 10^{-4}$ the ^{19}F abundance showed variation upto 46%. Thus it is likely that at higher values of T_9 the distribution of the elements gets shifted in such a way that the abundance of ^{19}F has shown to be such. Most likely the distribution takes place amongst the other elements in the cycle. Then again $^{19}F(p,\gamma)^{20}$Ne may also be a quiet influencial reaction at high temperature since it can then compete with $^{19}F(p,\alpha)^{16}$O. Moreover, as stated earlier, at larger temperature the ^{19}F destruction via (p,α) reaction deviates from non-resonant to behaviour which in turn makes an increment in destruction rate of ^{19}F. Now this abundance by mass fraction of ^{19}F and the hydrogen mass fractions at which ^{19}F's mass fractions are obtained are used to calculate the abundance of ^{19}F using the Eq.(5.1)

$$\varepsilon(F^{19}) = log\left[\frac{N(F^{19})}{N(H)}\right] + 12 \tag{5.1}$$

In Appendix D the observed and the estimated abundances of ^{19}F for all the metal poor stars of M4 reported in (Smith et al. 2005[288]), M22 in (Alves-Brito et al. 2012[275]) and 47 Tuc along with NGC 6397 in (de Laverny et al. 2013[276]) along with the difference between the observed and the calculated abundances are shown in the last column for each GCs. The Fig.(5.3) shows the comparative view of the tabulated values of both the calculated and observed abundances of the metal poor stars of the four clusters against the respective $[Fe/H]$ values. The $[Fe/H]$ values used here are the $[Fe^I/H]$ values directly taken from the respective authors except for M4. In the case of M4 the reported values of $\varepsilon(Fe)$ are first

converted into their respective $[Fe/H]$ values by the equation $[Fe/H] = \varepsilon(Fe) - \varepsilon(Fe)_{\odot}$ with $\varepsilon(Fe)_{\odot} = 7.45$. In the same figure the filled circles are values obtained from literature and open cirles are the values, calculated from this work.

5.3.2 Na-F (anti-) correlation

Although F measurements are available for only small samples of star and they exhibit star-to-star variations within the GCs, the data available for some GCs suggest a Na-F anticorrelation. In the figure the filled circles are values obtained from literature and open cirles are the values, calculated from this work. The top left panel of the Fig.(5.4) shows the ^{19}F abundance both calculated and observed are plotted against the observed ^{23}Na abundance reported in (Smith et al. 2005[288]) for GC M4 and the same reported in (Alves-Brito et al. 2012[275]) for GC M22 (top right panel) respectively, which shows clearly the anticorrelated behaviour between ^{19}F and ^{23}Na. Then in the bottom left panel the trend of anticorrelated behaviour between the calculated abundance of ^{19}F and the observed abundance of ^{23}Na reported in (de Laverny et al. 2013[276]) is also seen in the NGC 6397 for considered sample size. Here we have plotted the $\varepsilon(F^{19})$ for star III-12 and III-14 of GC M22 #68039 of 47 Tuc and all of NGC 6397 to be the maximum one as tabulated. However the same trend has not been seen between the estimated and observed abundances of ^{19}F and ^{23}Na in the selected sample of the 47 Tuc which is consistent with the report given by (de Laverny et al. 2013[276]). The abundance of ^{23}Na is calculated by the following equation

$$\varepsilon(Na^{23}) = \left[\frac{Na}{Fe}\right] + \left[\frac{Fe}{H}\right] + 6.17 \tag{5.2}$$

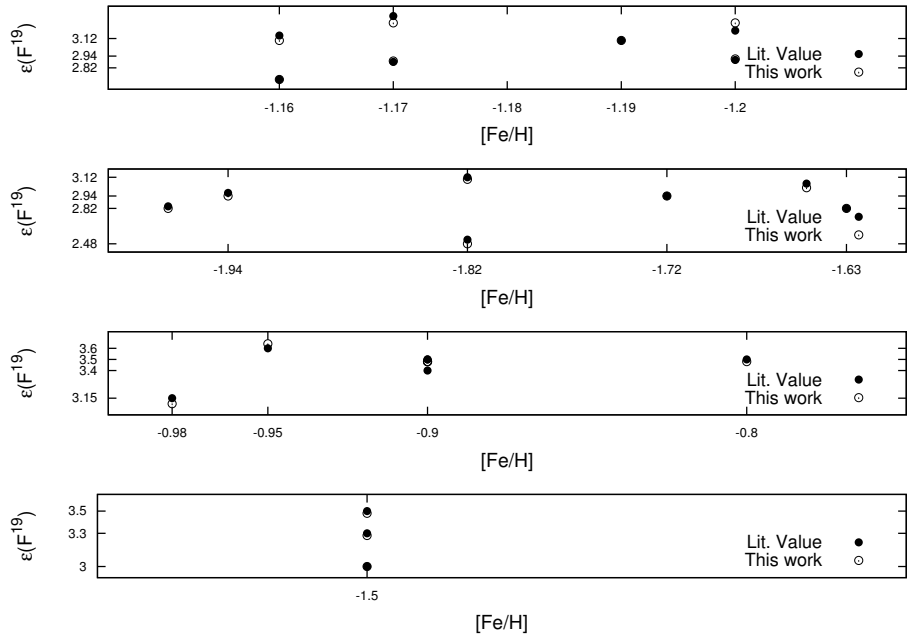

Fig. 5.3 This figure shows a comparative view of calculated and observed values of abundances.

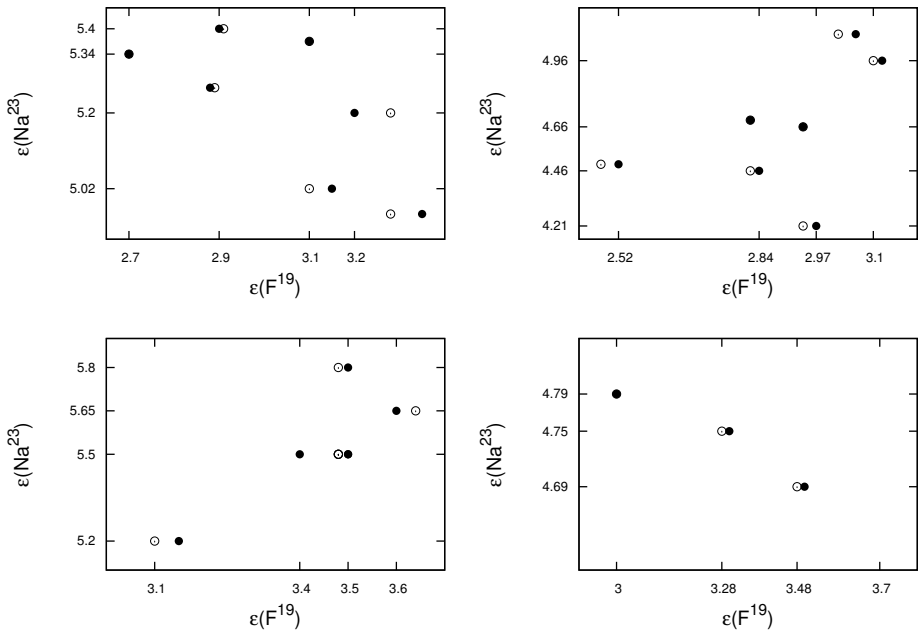

Fig. 5.4 This figure shows the signs of (anti)correlation between ^{19}F and ^{23}Na.

5.4 Summary

The origin of the abundance pattern and also the (anti)correlation present among the elements found in stars of globular clusters remains unimproved until date. The proton-capture reactions are presently recognised in concert of the necessary candidates for that sort of observed behaviour in the second generation stars. We tend to propose a reaction network of a nuclear cycle namely CNOF at evolved stellar condition since fluorine (^{19}F) is one such element which gets plagued by proton capture reactions. The stellar temperature thought about here ranges from 2×10^7 to 10×10^7 K and there has been an accretion occuring, with material density being 10^2 g/cm^3 and 10^3 g/cm^3. Such kind of temperature density conditions are probably going to be prevailing within the H-burning shell of evolved stars. The estimated abundances of ^{19}F are then matched with the info that has been determined for a few some metal-poor giants of GC M4, M22, 47 Tuc as well as NGC 6397. As far as the comparison between the observed and calculated abundances is concerned it's found that the abundance of ^{19}F have shown an excellent agreement with the observed abundances with a correlation coefficent above 0.9, supporting the incidence of that nuclear cycle at the adopted temperature density conditions.